

# Soft Matter

Accepted Manuscript



This is an Accepted Manuscript, which has been through the Royal Society of Chemistry peer review process and has been accepted for publication.

Accepted Manuscripts are published online shortly after acceptance, before technical editing, formatting and proof reading. Using this free service, authors can make their results available to the community, in citable form, before we publish the edited article. We will replace this Accepted Manuscript with the edited and formatted Advance Article as soon as it is available.

You can find more information about Accepted Manuscripts in the [author guidelines](#).

Please note that technical editing may introduce minor changes to the text and/or graphics, which may alter content. The journal's standard [Terms & Conditions](#) and the ethical guidelines, outlined in our [author and reviewer resource centre](#), still apply. In no event shall the Royal Society of Chemistry be held responsible for any errors or omissions in this Accepted Manuscript or any consequences arising from the use of any information it contains.

# Heterogeneity of crowded cellular fluids on the meso- and nanoscale

Olivia Stiehl and Matthias Weiss

*Experimental Physics I, University of Bayreuth, Universitätsstr. 30, D-95440 Bayreuth, Germany*

Cellular fluids are complex media that are crowded with macromolecules and membran-enclosed organelles on several length scales. Many studies have shown that crowding can significantly alter transport and reaction kinetics in biological but also in bio-mimetic fluids. Yet, experimental insights on how well bio-mimetic fluids can capture the complexity of cellular fluids are virtually missing. Therefore, we have combined fluorescence correlation spectroscopy (FCS) and fluorescence lifetime imaging microscopy (FLIM) to compare the spatial heterogeneities of biological and simple bio-mimetic crowded fluids. As a result, we find that these artificial fluids are capable of mimicking the average diffusion behavior but not the considerable heterogeneity of cellular fluids on the mesoscale (100 nm). On the nanoscale, not even the average properties are captured. Thus, cellular fluids feature a distinct, heterogeneous crowding state that differs from simple bio-mimetic fluids.

PACS numbers: 05.60.-k, 87.16.dj, 61.25.H-

**Introduction.** Cellular fluids are crowded with a plethora of macromolecules and membran-enclosed organelles. These structures span a wide range of sizes (1-500 nm) and hence can be expected to influence transport properties, e.g. diffusion coefficients, on multiple length and time scales. Indeed, slowed-down and anomalous diffusion, i.e. a nonlinear scaling of the mean square displacement of diffusing particles ( $\langle r(t)^2 \rangle \sim t^\alpha$  with  $\alpha < 1$ ), have been reported for biological and artificial crowded fluids [1–3]. Dividing cells even feature an anisotropic anomalous diffusion [4]. However, if and to which extent artificial crowded fluids can mimic the complexity of native, biological fluids like the cytoplasm has been poorly explored so far.

Moreover, almost all experimental studies have been focusing on mean transport coefficients (averaged over time and/or different loci) to explore the effects of crowding, that is, crowded fluids were tacitly supposed to be homogenous. Yet, this assumption appears debatable when bearing in mind that already very simple solutions with moderate levels of macromolecules can show significant spatial heterogeneities [5]. Furthermore, the degree of crowding, i.e. the apparent occupied volume fraction  $\phi$ , may vary between different length scales, in particular when considering biological specimen. Probing the crowding state only via diffusion measurements therefore appears inadequate as this approach is inherently based on averaging over extended particle trajectories (typically  $\sim 100$  nm), i.e. crowding on the nanoscale is masked by spatial averaging. In fact, the heterogeneity and multi-scale nature of crowding and the resulting differential impact on transport processes has been widely neglected in experiments so far. As a consequence, it has remained unclear if and to which extent artificial crowded fluids are appropriate to mimic, for example, the cytoplasm on those length scales that are relevant for typical biochemical reactions. The urgent demand for experimental data on the heterogeneity of crowding are further underlined by a variety of related theoretical ap-

proaches and model systems (see, for example, [6] for a review and [7, 8] for specific scenarios).

Here, we have combined fluorescence correlation spectroscopy (FCS) on fluorescently tagged macromolecules and fluorescence lifetime imaging (FLIM) on a soluble molecular rotor dye to explore the heterogeneity of crowded fluids on length scales  $\sim 1$  nm and  $\sim 100$  nm. In particular, we have determined the variation of diffusion times and anomalies, and fluorescence lifetimes in crowded fluids *in vitro*, in purified cytosol, and in the cytoplasm and nucleoplasm of living cells. From these data, we have derived estimates for the heterogeneity of the local occupied volume fraction,  $\phi$ . As a result, we find that simple artificial crowded fluids can represent the average diffusion behavior but not the marked heterogeneity of cellular fluids on the mesoscale ( $\sim 100$  nm). On the nanoscale, neither the average behavior nor the heterogeneity of cellular fluids are captured well. Hence, cellular fluids feature distinct local fluctuations of the volume occupancy, i.e. they provide a qualitatively and quantitatively special type of crowding that is not covered well by commonly used bio-mimetic fluids.

**Materials and Methods.** Artificial fluids crowded with PEG (polyethylene glycol, 10 kDa) or dextran (70 kDa) at a concentration of 30% weight per volume were based on MilliQ water or TE-buffer (10 mM Tris, 1 mM EDTA, 100 mM NaCl, pH 7.5). For FLIM experiments we have used DASPMI as a molecular rotor. Transparent cytosol from *Xenopus laevis* was purified as described before [9]. HeLa cells were cultured and transfected with a low-expression plasmid for EGFP [4]; microscopy was performed in ibidi 8-well chambers. Please see the Supplementary Information for details on the experiments and on the evaluation procedures.

**Results and Discussion.** Based on the standard definition of the signal-to-noise ratio, we have defined the heterogeneity of an observable  $x$  as the ratio of its stan-

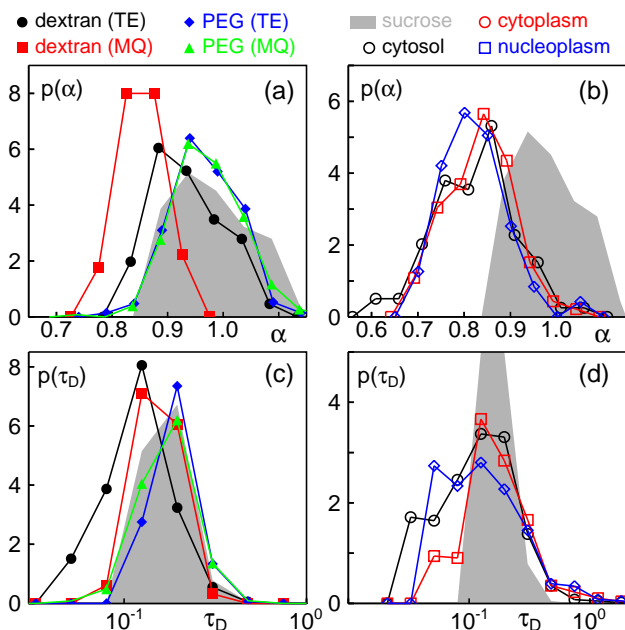


FIG. 1: (a) Probability distribution  $p(\alpha)$  of the diffusion anomaly of DASPMI in artificial fluids crowded with sucrose, PEG, or dextran using MilliQ water (MQ) or TE buffer (TE) as solvent. (b) Same for DASPMI in purified cytosol and for EGFP in the cytoplasm or nucleoplasm of living cells. Data for sucrose solutions are replicated for better comparison. (c,d) Corresponding distributions of diffusion times,  $p(\tau_D)$ , show a considerable broadening for cellular fluids that is also reflected in an approximate doubling of the associated heterogeneity values [Eq. (1)]:  $\eta(\tau_D) = 29.07\%$ ,  $24.71\%$ ,  $42.66\%$ ,  $31.90\%$ ,  $26.42\%$  for sucrose, dextran (MQ, TE), and PEG (MQ, TE), as compared to  $\eta(\tau_D) = 96.86\%$ ,  $121.15\%$ ,  $118.49\%$  for cytosol, cytoplasm, and nucleoplasm. Statistical uncertainties ('error bars') in  $\tau_D$  and  $\alpha$  for individual FCS experiments determine the minimum widths of  $p(\alpha)$  and  $p(\tau_D)$  for homogenous artificial fluids, i.e. biological fluids are markedly more heterogeneous (see also main text).

dard deviation and its mean:

$$\eta(x) = \frac{|dx|}{\langle x \rangle} = \frac{\sqrt{\langle (x - \langle x \rangle)^2 \rangle}}{\langle x \rangle}. \quad (1)$$

Certainly, Eq. (1) only reflects some aspects of the observable's probability distribution,  $p(x)$ , yet it is a straightforward way to compare fluctuations of  $x$  in different samples via a single number. Moreover, starting from the heterogeneity of experimentally accessible observables from FCS and FLIM, the definition of  $\eta$  allows us to estimate the heterogeneity of the local volume occupancy,  $\eta(\phi)$ , on the nano- and mesoscale.

As a first step, we aimed at exploring heterogeneities of crowded fluids on scales that are accessible via diffusion measurements ( $\sim 100$  nm). Following previous work [10], we therefore used FCS to reveal spatial variations of the diffusion of a tracer particle in the following samples (see

Supplementary Information for details): (i) artificial fluids with dextran or PEG as crowding agents, using MilliQ water or TE buffer as solvents, (ii) purified cytosol, and (iii) intracellular fluids (cytoplasm and nucleoplasm) *in vivo*. In each sample, we acquired a large number of FCS curves at different locations and extracted for each curve the diffusion time,  $\tau_D$ , and anomaly,  $\alpha$ , via fitting. Please note that crowding-induced diffusion anomalies typically vanish for length and time scales beyond those accessible to FCS experiments [11]. As a result, we observed very similar probability distribution functions  $p(\alpha)$  for sucrose- and PEG-crowded fluids (Fig. 1a) with a vanishing mean anomaly ( $\langle \alpha \rangle \approx 0.97$ ), whereas dextran-crowded fluids featured a solvent-dependent diffusion anomaly (MQ:  $\langle \alpha \rangle = 0.85$ ; TE:  $\langle \alpha \rangle = 0.93$ ) in agreement with previous observations [12]. Values  $\eta(\alpha)$  associated with these supposedly homogenous solutions (Table I) suggest a threshold  $\eta_c(\alpha) = 7\%$  below which  $\eta(\alpha)$  indicates mere statistical uncertainties of  $\alpha$  due to the fitting process rather than reporting a true heterogeneity of the fluid. Indeed, fitting FCS curves with mean anomalies in the range  $0.8 \leq \langle \alpha \rangle \leq 1$  is associated with an uncertainty  $\langle \alpha \rangle \pm 0.05$  [13], leading to a similar threshold criterion. Using  $\eta_c(\alpha) = 7\%$  as a threshold, purified cytosol indeed appears to feature an appreciable heterogeneity ( $\eta(\alpha) \approx 10.6\%$ , Table I) with a slightly stronger mean anomaly ( $\langle \alpha \rangle = 0.82$ , see Fig. 1b). Further support to a non-trivial heterogeneity in cytosol is obtained when inspecting the distributions of diffusion times,  $p(\tau_D)$  (Fig. 1c,d): The heterogeneity value for cytosol  $\eta(\tau_D) \approx 97\%$  is about twice as high as the largest value obtained for artificial fluids (dextran in TE buffer,  $\eta(\tau_D) = 42.66\%$ ). We therefore conclude that purified cytosol indeed shows a significant heterogeneity.

In order to compare these findings to diffusion data in living cells, we used EGFP as a diffusion probe since DASPMI's intracellular fluorescence yield was too poor to obtain FCS curves that were smooth enough to be fitted with satisfactory accuracy. However, a superposition of FCS curves on DASPMI and EGFP *in vivo* showed no systematic deviations between both tracers, i.e. EGFP probes the same length and time scales as DASPMI. Indeed, probability distribution functions  $p(\alpha)$  found for cytoplasm and nucleoplasm are centered around  $\langle \alpha \rangle = 0.82$  and  $\langle \alpha \rangle = 0.83$ , respectively, and hence compare favorably to data seen for DASPMI in purified cytosol (see Fig. 1b). As compared to purified cytosol,  $p(\alpha)$  was narrower for cytoplasm and nucleoplasm, resulting in lower heterogeneity values ( $\eta(\alpha) \approx 8.5\%$ , cf. Table I). While these values are still above the chosen threshold  $\eta_c(\alpha)$ , one may debate whether they report a true heterogeneity of the fluids. Yet, the corresponding distributions of diffusion times (Fig. 1d) and the associated heterogeneities  $\eta(\tau_D) \approx 120\%$  highlight a substantial difference between these cellular fluids and their artificial counterparts ( $\eta(\tau_D) \leq 43\%$ ). We therefore conclude

that cytoplasm and nucleoplasm, like cytosol, feature significant heterogeneities.

Based on the marked heterogeneity  $\eta(\alpha)$  found in cytosol, cytoplasm, and nucleoplasm, we aimed at extracting an estimate for the heterogeneity of the apparent occupied volume fraction,  $\eta(\phi)$ , on the mesoscale. Since the diffusion anomaly has been shown earlier to depend almost linearly on the concentration of crowders [13], it appears reasonable to assume a relation  $\alpha = 1 - c\phi$ . Using  $\alpha = 0.8$ , we obtain via standard differential calculus

$$\eta(\alpha) = \frac{c\langle\phi\rangle}{1 - c\langle\phi\rangle} \eta(\phi) \approx \frac{1}{4} \eta(\phi). \quad (2)$$

Thus, the apparent heterogeneity of the occupied volume fraction on length scales accessible via diffusion measurements is in the range  $\eta(\phi) \approx 33 - 43\%$  for cytosol and intracellular fluids (cf. Table I).

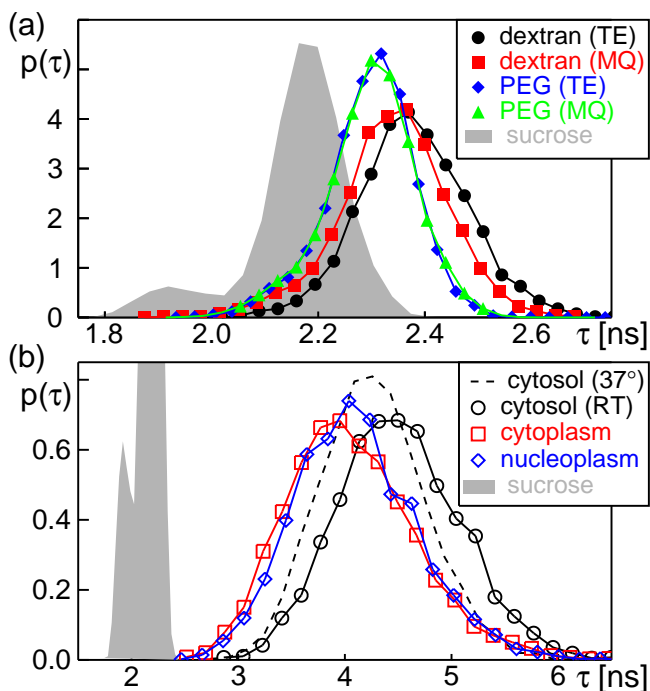


FIG. 2: (a) Probability distribution  $p(\tau)$  of averaged fluorescence lifetimes,  $\tau$ , obtained for DASPMI at different locations in artificial fluids crowded with sucrose, PEG, or dextran. Using MilliQ water (MQ) or TE buffer (TE) as solvent yielded similar results, indicating a negligible impact of salt conditions on  $p(\tau)$  and  $\eta(\tau)$ . (b) Same for purified cytosol (at room temperature, RT, and at 37°C), and in the cytoplasm or nucleoplasm of living cells (at 37°C). Data for sucrose solutions are replicated for better comparison. Minor differences of cytosol's  $p(\tau)$  between RT and 37°C indicate a negligible influence of temperature on  $\eta(\tau)$ .

Next, we performed FLIM on the fluorescent molecular rotor DASPMI at different locations in the samples to probe their heterogeneity on the nanoscale (see

Supplementary Information for details). Molecular rotors report on a varying local environment, e.g. on viscosity and polarity, by adapting their fluorescence lifetime [14, 15]. Unlike the majority of molecular rotors, DASPMI is water-soluble and autonomously partitions into all subcellular fluids of living cells [16]. In contrast to FCS, evaluation of our pixel-wise acquired FLIM data did not require fitting of any theoretical expression. Rather, the mean and standard deviation of the fluorescence lifetimes over all pixels within the respective compartment (e.g. the nucleoplasm) could be calculated directly after background correction (see Supplementary Information). Background events reflect noise in the photodiode, i.e. few spontaneous counts are uniformly distributed between two excitation pulses whereas fluorescence photons emitted by DASPMI show a peaked distribution with a mean of few nanoseconds (see example curves in the Supplementary Information). To inspect the spatial heterogeneity, we calculated in each pixel the average lifetime of DASPMI,  $\tau$ , and inspected then the probability distribution of times from all pixels,  $p(\tau)$ , to determine  $\eta(\tau)$ .

As a result, we observed very narrow distributions  $p(\tau)$  in artificial crowded fluids with a mean lifetime  $\langle\tau\rangle \approx 2.3$  ns (Fig. 2a). In contrast,  $\langle\tau\rangle$  in cytosol (at room temperature and at 37°C), and in the cytoplasm and nucleoplasm of living cells (kept at 37°C) was about two-fold higher (Fig. 2b). Moreover, the width of  $p(\tau)$  was significantly larger, indicating a very different crowding state in biological fluids. In order to obtain a lower bound  $\eta_0(\tau)$  for the lifetime's heterogeneity, we inspected the changes of  $\eta(\tau)$  in artificial solutions when varying the number of photons per pixel,  $n_p$ , used for calculating the average local fluorescence lifetime. In line with our prediction for a homogenous solution with exponentially distributed lifetimes we observed  $\eta(\tau) \sim 1/\sqrt{n_p}$  for artificial solutions when using  $n_p = 25, 50, 100, 200$  photons per pixel for averaging. This indicates that heterogeneities observed in the artificial fluids are solely due to statistics, i.e. they were deemed homogenous also on the nanoscale. This conclusion is corroborated by FLIM data on homogenous sucrose solutions (40% weight per volume) for which we observed similar data for  $p(\tau)$  (cf. Fig. 2a) yielding  $\eta(\tau) \approx 4.6\%$  at  $n_p = 25$ . Focusing on  $n_p = 25$  photons per pixel for all subsequent evaluations, we have therefore set  $\eta_0(\tau) = 5\%$  as a threshold, i.e. artificial crowded fluids were deemed to not show a significant heterogeneity of lifetimes (Table I). In contrast, cytosol (at room temperature and at 37°C) and intracellular fluids featured heterogeneities  $\eta(\tau) > \eta_0(\tau)$  *in vivo* (cf. Table I), indicating a distinct crowding state of these biological fluids on the nanoscale.

Aiming at extracting the nanoscale heterogeneity of the occupied volume fraction,  $\eta(\phi)$ , from these data, we focused on the empirical scaling  $\tau \sim \sqrt{\mu}$  of a molecular rotor's lifetime in a solution of viscosity  $\mu$  (Ref. [14]). Approximating crowded fluids to behave similar to dense

Supplementary Information for details). Molecular rotors report on a varying local environment, e.g. on viscosity and polarity, by adapting their fluorescence lifetime [14, 15]. Unlike the majority of molecular rotors, DASPMI is water-soluble and autonomously partitions into all subcellular fluids of living cells [16]. In contrast to FCS, evaluation of our pixel-wise acquired FLIM data did not require fitting of any theoretical expression. Rather, the mean and standard deviation of the fluorescence lifetimes over all pixels within the respective compartment (e.g. the nucleoplasm) could be calculated directly after background correction (see Supplementary Information). Background events reflect noise in the photodiode, i.e. few spontaneous counts are uniformly distributed between two excitation pulses whereas fluorescence photons emitted by DASPMI show a peaked distribution with a mean of few nanoseconds (see example curves in the Supplementary Information). To inspect the spatial heterogeneity, we calculated in each pixel the average lifetime of DASPMI,  $\tau$ , and inspected then the probability distribution of times from all pixels,  $p(\tau)$ , to determine  $\eta(\tau)$ .

As a result, we observed very narrow distributions  $p(\tau)$  in artificial crowded fluids with a mean lifetime  $\langle\tau\rangle \approx 2.3$  ns (Fig. 2a). In contrast,  $\langle\tau\rangle$  in cytosol (at room temperature and at 37°C), and in the cytoplasm and nucleoplasm of living cells (kept at 37°C) was about two-fold higher (Fig. 2b). Moreover, the width of  $p(\tau)$  was significantly larger, indicating a very different crowding state in biological fluids. In order to obtain a lower bound  $\eta_0(\tau)$  for the lifetime's heterogeneity, we inspected the changes of  $\eta(\tau)$  in artificial solutions when varying the number of photons per pixel,  $n_p$ , used for calculating the average local fluorescence lifetime. In line with our prediction for a homogenous solution with exponentially distributed lifetimes we observed  $\eta(\tau) \sim 1/\sqrt{n_p}$  for artificial solutions when using  $n_p = 25, 50, 100, 200$  photons per pixel for averaging. This indicates that heterogeneities observed in the artificial fluids are solely due to statistics, i.e. they were deemed homogenous also on the nanoscale. This conclusion is corroborated by FLIM data on homogenous sucrose solutions (40% weight per volume) for which we observed similar data for  $p(\tau)$  (cf. Fig. 2a) yielding  $\eta(\tau) \approx 4.6\%$  at  $n_p = 25$ . Focusing on  $n_p = 25$  photons per pixel for all subsequent evaluations, we have therefore set  $\eta_0(\tau) = 5\%$  as a threshold, i.e. artificial crowded fluids were deemed to not show a significant heterogeneity of lifetimes (Table I). In contrast, cytosol (at room temperature and at 37°C) and intracellular fluids featured heterogeneities  $\eta(\tau) > \eta_0(\tau)$  *in vivo* (cf. Table I), indicating a distinct crowding state of these biological fluids on the nanoscale.

Aiming at extracting the nanoscale heterogeneity of the occupied volume fraction,  $\eta(\phi)$ , from these data, we focused on the empirical scaling  $\tau \sim \sqrt{\mu}$  of a molecular rotor's lifetime in a solution of viscosity  $\mu$  (Ref. [14]). Approximating crowded fluids to behave similar to dense

colloidal suspensions with a viscosity  $\mu \sim 1 + 2.5\phi + 6\phi^2$  (Ref. [17]) yields:

$$\eta(\tau) = \frac{1.25\langle\phi\rangle + 6\langle\phi\rangle^2}{1 + 2.5\langle\phi\rangle + 6\langle\phi\rangle^2}\eta(\phi). \quad (3)$$

Using  $\langle\phi\rangle = 0.3$  (Ref. [18]), we obtain  $\eta(\tau) \approx 0.4\eta(\phi)$  from our FLIM data. This estimate indicates  $\eta(\phi) \approx 31 - 38\%$  on the nanoscale for purified cytosol and intra-cellular fluids (Table I). Hence, based on both estimates, cellular fluids feature comparable heterogeneities on the meso- and nanoscale (cf. columns 3 and 5 in Table I). In fact, deviations between both estimates could indicate that cellular fluids appear more or less well-mixed on the respective length scale.

In summary, our FCS and FLIM data indicate a considerable heterogeneity of the occupied volume fraction in cellular fluids that is not captured by simple biomimetic fluids: While the average diffusion behavior on the mesoscale is reflected to a reasonable extent, considerable differences are seen on the nanoscale. Thus, crowding of biological fluids needs to be viewed as a somewhat more complex and heterogeneous phenomenon than discussed in the literature so far.

Our finding that cellular fluids feature marked spatial fluctuations in the apparent occupied volume fraction on scales of  $\sim 1$  nm and  $\sim 100$  nm) might suggest a self-similar texture of these fluids at each instant of time. Indeed, unlike their virtually homogenous artificial counterparts, cellular fluids contain organelles and macromolecular structures of grossly varying size, hence texturing the specimen in complex fashion. While interfacial water in this multi-scale crowded environment may affect the apparent molecular mobility on small scales, protein complexes and organelle structures may set up a self-similar maze of impenetrable obstacles on larger scales. As a consequence, dye molecules performing a random walk in this setting will report on strongly varying local environments on multiple scales, giving rise to the observed spatial heterogeneity of FLIM and FCS data. In support of this picture, recent simulations on percolation-like random fractal geometries have highlighted a significant spatial heterogeneity of the diffusion of tracers due to the random occurrence of isolated islands with lower/higher obstacle density [19].

While being inhomogeneous at each instant of time, ergodicity requires also cellular fluids to dynamically overturn their texture. Aiming at exploring the spatial heterogeneity via local FCS/FLIM measurements therefore requires the measurement time per locus to be short with respect to the correlation time of the texture change. Given that the motion of larger cytoplasmic structures via diffusion is on the scale of many minutes, our data acquisition was just rapid enough to assess the heterogeneity. It will be interesting to complement our findings with faster or multiplexed experimental methods, and

also to utilize simulations to gain a deeper understanding of the dynamic organization of cellular fluids.

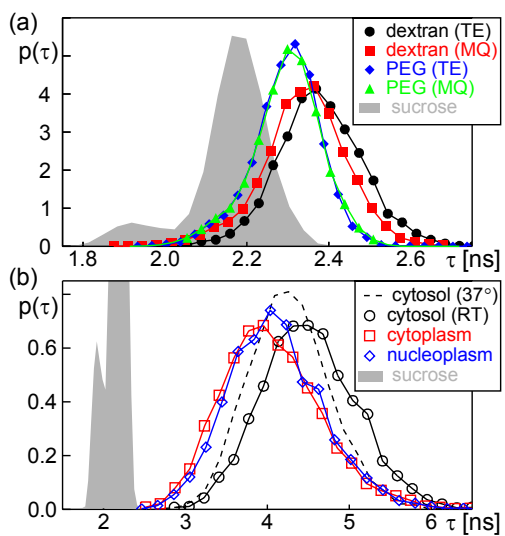
TABLE I: Summary of experimentally determined heterogeneities. Columns 2 and 3 report FCS-based data (mesoscale, cf. Eq. (2)), columns 4 and 5 display FLIM-based data (nanoscale, cf. Eq. (3)).

	$\eta(\alpha)$	$\eta(\phi)$	$\eta(\tau)$	$\eta(\phi)$
sucrose (MQ)	6.90 %	-	4.61%	-
PEG (MQ)	6.46 %	-	3.78%	-
PEG (TE)	6.33 %	-	3.62%	-
dextran (MQ)	4.67 %	-	4.42%	-
dextran (TE)	6.90 %	-	4.30%	-
cytosol	10.65 %	42.60%	12.71%	31.78%
cytoplasm	8.75 %	35.00%	14.89%	37.23%
nucleoplasm	8.38 %	33.52%	14.12%	35.30%

**Acknowledgement.** We thank C.-M. Ferencz for providing an aliquot of purified cytosol, A. Veres for extracting the photon current from the Symphotime software, and G. van den Boogart for help with the reconstruction of FLIM images from raw binary data. Financial support from DFG grant WE4335/3-1 is gratefully acknowledged.

- 
- [1] J. Dix and A. Verkman, *Ann. Rev. Biophys.* **37**, 247 (2008).
  - [2] F. Höfling and T. Franosch, *Rep. Prog. Phys.* **76**, 046602 (2013).
  - [3] M. Weiss, *Int. Rev. Cell Mol. Biol.* **307**, 383 (2014).
  - [4] N. Pawar, C. Donth, and M. Weiss, *Curr Biol* **24**, 1905 (2014).
  - [5] H. R. Brand and K. Kawasaki, *Physica A* **324**, 484 (2003).
  - [6] R. Metzler, J.-H. Jeon, A. Cherstvy, and E. Barkai, *Phys. Chem. Chem. Phys.* **16**, 24128 (2014).
  - [7] S. Ghosh, A. Cherstvy, and R. Metzler, *Phys. Chem. Chem. Phys.* **17**, 1847 (2015).
  - [8] S. Ghosh, A. Cherstvy, D. Grebenkov, and R. Metzler, *New J. Phys.* **18**, 013027 (2016).
  - [9] C.-M. Ferencz, G. Guigas, A. Veres, B. Neumann, O. Stemmann, and M. Weiss, *BBA Biomembranes* **1858**, 2035 (2016).
  - [10] J. Szymanski and M. Weiss, *Phys. Rev. Lett.* **103**, 038102 (2009).
  - [11] D. Ernst, M. Hellmann, J. Köhler, and M. Weiss, *Soft Matt.* **8**, 4886 (2012).
  - [12] O. Stiehl, K. Weidner-Hertrampf, and M. Weiss, *Phys. Rev. E* **91**, 012703 (2015).
  - [13] M. Weiss, M. Elsner, F. Kartberg, and T. Nilsson, *Biophys. J.* **87**, 3518 (2004).
  - [14] M. K. Kuimova, G. Yahioglu, J. A. Levitt, and K. Suhling, *JACS* **130**, 6672 (2008).
  - [15] J. M. Nolle, C. Jungst, A. Zumbusch, and D. Woll, *Polym. Chem.* **5**, 2700 (2014).
  - [16] R. Ramadass and J. Bereiter-Hahn, *Biophys J* **95**, 4068 (2008).

- [17] R. Verberg, I. M. de Schepper, and E. G. D. Cohen, Phys. Rev. E **55**, 3143 (1997).
- [18] R. Ellis, Trends Biochem. Sci. **26**, 597 (2001).
- [19] Y. Mardoukhi, J.-H. Jeon, and R. Metzler, Phys. Chem. Chem. Phys. **17**, 30134 (2015).



Advanced light microscopy methods reveal that crowded cellular fluids feature a distinct, heterogeneity that differs significantly from simple bio-mimetic fluids.